Tunable flat-band slow light via contra-propagating cavity modes in twin coupled microresonators

Ang, Thomas Y. L.; Ngo, Nam Quoc

2012

Ang, T. Y. L. & Ngo, N. Q. (2012). Tunable flat-band slow light via contra-propagating cavity modes in twin coupled microresonators. Journal of the Optical Society of America B, 29(5), 924-933.

https://hdl.handle.net/10356/79773

https://doi.org/10.1364/JOSAB.29.000924

Tunable flat-band slow light via contra-propagating cavity modes in twin coupled microresonators

Thomas Y. L. Ang* and Nam Quoc Ngo

Photonics Research Center, School of Electrical and Electronic Engineering, Nanyang Technological University, 50 Nanyang Avenue, Singapore, 639798, Singapore
**Corresponding author: thomas@pmail.ntu.edu.sg*

Received September 27, 2011; revised January 6, 2012; accepted January 6, 2012; posted January 24, 2012 (Doc. ID 155247); published April 6, 2012

We utilize the contra-propagating cavity modes that arise from the evanescent coupling of both the resonators to the bus waveguide in a twin coupled traveling-wave microresonators (MRs) system to generate flat-band slow light (SL). The contra-propagating cavity modes will generate multipeaks in the resonance spectra. Flat-band SL can be generated if such multipeaks become undistinguishable and merge into one single broadened peak that is maximally flat when the inter-resonator coupling strength is optimized relative to the resonators-to-bus-waveguide coupling strengths. The bandwidth and the group delay can be tuned by adjusting the coupling strengths. It is shown that the delay-bandwidth products of the output light at the through (reflection) port are 3- to 12-fold (6- to 24-fold) higher than that of conventional MR-based SL systems. Fabrication tolerance and cavity losses analyses have also revealed that the proposed scheme is rather robust to the fabrication errors and limitations of current state-of-the-art semiconductor processing technology.

OCIS codes: 130.2790, 130.3120, 230.4555, 230.5750, 230.7020.

1. INTRODUCTION

Slow light (SL) holds the key to increase the speed of optical communications [1] as it offers the abilities in delaying, coherently stopping, and storing data trains [2], which are needed for enhanced performances in optical networks. The most simple and compact scheme to generate SL in traveling-wave microresonators (MRs) can be achieved in one of two ways. The first way is by resonance enhancement via one single MR—the group delay t_g is increased by forcing the light to circulate many times in the MR. In this case, the MR can be either coupled to one bus waveguide (WG) [3,4], which we will term as the 1-cavity-1-bus configuration, or to two bus WGs [5,6], which we will term as the 1-cavity-2-buses configuration. The second way is by optically mimicking the atomic concept of electromagnetically induced transparency (EIT) [7]—this is known as coupled-resonator-induced transparency (CRIT) and is typically realized by coupling two MRs together [8–11] such that the coupled MRs behave like atoms with EIT settings.

A practical SL system should ideally have (1) a large t_g enhancement and (2) flat or minimal dispersion in the t_g and transmission T spectra (with transmission $T \approx 1$) over a large usable resonance bandwidth Δf_u. To quantify criteria (1) and (2), we use the delay-bandwidth product (DBP), which is defined as $\mathrm{DBP} = t_{gm} \times \Delta f_u \approx$ constant [12], where t_{gm} is the maximum group delay at resonance. The DBPs of the above-mentioned resonance enhancement scheme are computed to be $\sim 2/\pi$ and $\sim 1/(2\pi)$ for the 1-cavity-1-bus and 1-cavity-2-buses configurations, respectively, while that of the above-mentioned CRIT scheme with a two coupled MRs is $\sim 1/\pi$. These DBPs are computed using the full width at half maximum (FWHM) as the usable resonance bandwidth Δf_u. In reality, to minimize higher-order dispersion, $\Delta f_u \ll$ FWHM. This implies lower DBPs than the above computed figures. A lower DBP generally means that a large group delay t_g results in a much smaller usable resonance bandwidth Δf_u. This will restrict the use of these SL media in transmission systems with ultrashort pulses. Though cascading multiple MRs (or unit cells) [12–18] will increase t_g, the DBP remains approximately the same as that of a single MR in the resonance enhancement scheme [3–6] or the twin coupled MRs in the CRIT scheme [8–11] due to the formation of ripples in the resonance spectra that will distort the signal and consequently reduce Δf_u.

In this work, we look into the use of a twin coupled MRs scheme (cf. Fig. 1) to realize an SL system that has sufficiently large group delay t_g and high transmission T, with minimal dispersion in t_g and T over a wide bandwidth (i.e., flat-band SL with enhanced DBPs). As shown in Table 1, the proposed scheme improves the DBP by 3- to 24-fold as compared to conventional MR-based SL systems [3–6,8–18]. Though our scheme is similar to [9,19,20], the analyses in these works are chiefly limited to the filtering characteristics, without a detailed study of the SL performances. Also, note that our twin coupled MRs are different from that in [8,10,11,21], which have only one MR directly coupled to the bus WG, while both the MRs are directly coupled to the bus WG in this work.

This work is arranged as follows. In Section 2, we present the theoretical modeling of the proposed scheme. In Section 3, the physical mechanism behind the generation of the flat-band SL is illustrated. This is followed by a characterization of the performances of the flat-band SL in Section 4. In Section 5, we analyze the loss sensitivity of the proposed scheme. Finally, we conclude in Section 6.

2. THEORETICAL FORMULATION

The proposed twin coupled MRs system is shown in Fig. 1, whereby two MRs, which are mutually coupled to each other, are both directly coupled to the port WG as well. This excites both clockwise (CW) and counterclockwise (CCW) cavity

modes. Note that all the components are single-moded in this work. In Fig. 1, the electric fields in each MR are represented by a_n^x, b_n^x, c_n^x, and d_n^x, where $x = -(x = +)$ denotes the CW (CCW) mode, while $n = 1$ ($n = 2$) denotes the left (right) MR. Likewise, the electric fields in the port WG are represented by A_n^x, B_n^x, C_n^x, and D_n^x, with $x = -(x = +)$ denoting the backward (forward) propagating mode, while $n = 1$ ($n = 2$) denotes the side of the WG located below the left (right) MR. The evanescent coupling between the MRs at coupling junction (CJ) 1 can be described as

$$[c_2^- \quad d_2^- \quad d_2^+ \quad c_2^+]^T = S_1[c_1^+ \quad d_1^+ \quad d_1^- \quad c_1^-]^T, \tag{1}$$

while the evanescent coupling between the MR and WG at CJs 2 and 3 can be written as

$$[a_1^- \quad b_1^- \quad b_1^+ \quad a_1^+]^T = S_2[A_1^- \quad B_1^- \quad B_1^+ \quad A_1^+]^T, \tag{2}$$

$$[A_2^+ \quad B_2^+ \quad B_2^- \quad A_2^-]^T = S_3[a_2^+ \quad b_2^+ \quad b_2^- \quad a_2^-]^T, \tag{3}$$

in which S_i ($i = 1$, 2, or 3) is termed as the coupling matrix that is defined as

$$S_i = \begin{pmatrix} [U_i] & 0 \\ 0 & [U_i] \end{pmatrix}, \quad \text{with}$$
$$U_i = \begin{pmatrix} r_i/(j\kappa_i) & -1/(j\kappa_i) \\ (\kappa_i^2 + r_i^2)/(j\kappa_i) & -r_i/(j\kappa_i) \end{pmatrix}, \tag{4}$$

where $j = \sqrt{-1}$, while r_i and κ_i are, respectively, the through and cross coupling coefficients. Do note that $k_i^2 + r_i^2 = 1 - \sigma_i^2$ represents the attenuation constant of the coupler at each CJ, in which σ_i quantifies for the coupler loss ($\sigma_i = 0$ for a lossless coupler). The subscript $i = 1$, 2, or 3 represents the position of the CJs in Fig. 1, where $i = 1$, 2, and 3 corresponds to CJ 1, CJ 2, and CJ 3, respectively. Within the MRs, the electric fields are described as

$$[c_1^+ \quad d_1^+ \quad d_1^- \quad c_1^-]^T = P_1[a_1^- \quad b_1^- \quad b_1^+ \quad a_1^+]^T, \tag{5}$$

$$[a_2^+ \quad b_2^+ \quad b_2^- \quad a_2^-]^T = P_2[c_2^- \quad d_2^- \quad d_2^+ \quad c_2^+]^T, \tag{6}$$

in which P_n ($n = 1$ or 2) is termed as the propagation matrix that is defined as

$$P_n = \begin{pmatrix} 0 & 0 & 0 & \tau_n^{1/4}\exp(j\delta_n/4) \\ 0 & 0 & \tau_n^{-3/4}\exp(-j3\delta_n/4) & 0 \\ 0 & \tau_n^{3/4}\exp(j3\delta_n/4) & 0 & 0 \\ \tau_n^{-1/4}\exp(-j\delta_n/4) & 0 & 0 & 0 \end{pmatrix}, \tag{7}$$

where τ_n is the round-trip amplitude transmission coefficient (lossless MR: $\tau_n = 1$) and $\delta_n = 2\pi R_n \beta_{R,n}$ is the round-trip phase shift, in which R_n and $\beta_{R,n}$ are, respectively, the bend radius and propagating constant of the MR, with $n = 1$ ($n = 2$) denoting the left (right) MR. The electric fields in the bus WG can be described as

$$[A_2^+ \quad A_2^-]^T = \begin{pmatrix} \exp(j\beta_w L_w) & 0 \\ 0 & \exp(-j\beta_w L_w) \end{pmatrix}[A_1^+ \quad A_1^-]^T, \tag{8}$$

where β_w and L_w are, respectively, the propagating constant of the bus WG and the separation distance between the MRs. Setting $B^-{}_2 = 0$ (i.e., only one input) and using Eqs. (1)–(8), the fields propagating in the bus WG can then be described as

$$[A_1^+ \exp(-j\beta_w L_w) \quad B_2^+ \quad 0 \quad A_1^- \exp(j\beta_w L_w)]^T = Y[A_1^- \quad B_1^- \quad B_1^+ \quad A_1^+]^T, \tag{9}$$

where $Y = S_3P_2S_1P_1S_2$ is a 4×4 matrix. We are interested to solve for $\xi_T = B^+{}_2/B^+{}_1$ and $\xi_R = B^-{}_1/B^+{}_1$, which are, respectively, the complex electric field transmissivities at the through and reflection ports. To do so, we recast Eq. (9) as

$$\begin{bmatrix} A_1^-/B_1^+ \\ B_1^-/B_1^+ \\ A_1^+/B_1^+ \\ B_2^+/B_1^+ \end{bmatrix} = \begin{bmatrix} Y_{11} & Y_{12} & Y_{14} - \exp(j\beta_w L_w) & 0 \\ Y_{21} & Y_{22} & Y_{24} & -1 \\ Y_{31} & Y_{32} & Y_{34} & 0 \\ Y_{41} - \exp(-j\beta_w L_w) & Y_{42} & Y_{44} & 0 \end{bmatrix}^{-1} \times \begin{bmatrix} -Y_{13} \\ -Y_{23} \\ -Y_{33} \\ -Y_{43} \end{bmatrix}. \tag{10}$$

In this work, ξ_T and ξ_R are collectively termed as ξ_q ($q = T$ or R), where the subscript $T(R)$ denotes the through (reflection) port. Note that ξ_q contains all the information needed to characterize the SL properties: $|\xi_q|^2$ gives the transmission T_q, while $\Phi_q = \arg(\xi_q)$ is the MR-induced effective phase shift of the output light that determines the group delay $t_{g,q}$, which can be defined as $t_{g,q} = t_{rt}\partial\Phi_q/\partial\delta$, where t_{rt} is the cavity round-trip time.

3. GENERATING FLAT-BAND SLOW LIGHT

A. General Operating Mechanism

To understand the operating mechanism behind the proposed scheme, it is instructive to first analyze a single MR system (i.e., only MR 1 exists in Fig. 1) [3,4] and a twin coupled MRs system that has only one cavity directly coupled to the bus WG (i.e., $\kappa_3 = 0$ in Fig. 1) [8,10,11]. We will assume that the losses of the MRs and couplers are negligible (i.e., $\tau_n = 1$ and $\sigma_n = 0$) in this section. For simplicity, only the case of coresonant cavities (i.e., $\delta_1 = \delta_2 = \delta$) is considered in this work. This will generate flat-band SL centered at the normalized resonance frequency $\delta = 2\pi m$ (where $m = 1, 2, 3\ldots$) if certain physical conditions (governed by Eq. (16), as derived later) are met.

For the single MR system, the complex transmissivity ξ_T has the expression $\xi_T = (\exp(j\delta) - r_2)/(r_2\exp(j\delta) - 1)$. Consequently, there is only one eigenmode that is resonant at $\delta = 2\pi m$. A sharp Lorentzian resonance lineshape is then

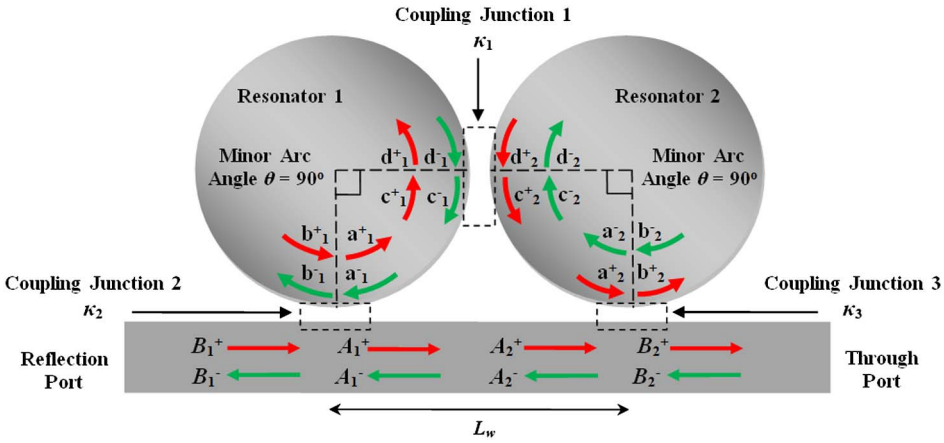

Fig. 1. (Color online) Schematic of the proposed twin coupled traveling-wave MRs.

formed at $\delta = 2\pi m$, as shown in the transmission and group delay spectra in Figs. 2(ai) and 2(aiii) in blue line plots, with a rapid phase shift of 2π across the resonance in Fig. 2(aii). The eigenmode (at $\delta = 2\pi m$) of the single MR system is denoted as δ_0. When a second MR is coupled to the single MR such that it is not directly coupled to the bus WG (i.e., $\kappa_3 = 0$ in Fig. 1), ξ_T becomes $\xi_T = (\xi_2 \exp(j\delta) - r_2)/(\xi_2 r_2 \exp(j\delta) - 1)$, where $\xi_2 = (\exp(j\delta) - r_1)/(r_1 \exp(j\delta) - 1)$ is the loading factor due to the addition of the second MR. This results in two eigenmodes δ_1 and δ_2 that can be approximated as

$$\delta_1 = \delta_0 - \sin^{-1}\kappa_1, \qquad \delta_2 = \delta_0 + \sin^{-1}\kappa_1, \tag{11}$$

where $\delta_0 = 2\pi m$ is the eigenmode of the above-mentioned single MR system. Thus, the resonance frequency δ_0 of the single MR is split into δ_1 and δ_2, with the mode splitting being controlled by κ_1. As a result, the resonance spectra have the shape of a two-split Lorentzian, as shown in Figs. 2(ai) and 2(aiii) in red line plots, with the effective phase shift being split into two 2π swings in Fig. 2(aii). Finally, if both MRs are coupled to the bus WG (i.e., $\kappa_3 \neq 0$) such that one has the proposed configuration in this work (cf. Fig. 1), contra-propagating cavity modes are excited. Then, both forward and backward transmissions, i.e., $T_T = |\xi_T|^2$ and $T_R = |\xi_R|^2$, are observed. Note that $r = r_2 = r_3$ and $\kappa = \kappa_2 = \kappa_3$. Using this and Eq. (10), the complex transmissivities ξ_T and ξ_R can be expressed as

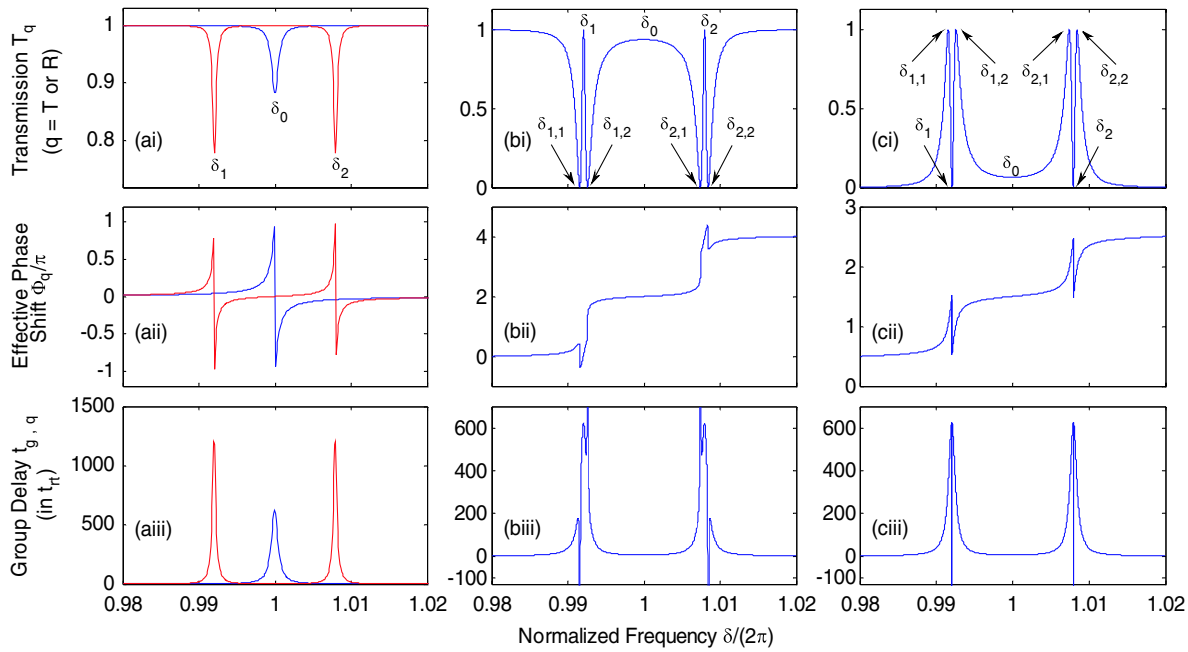

Fig. 2. (Color online) The transmission, effective phase shift, and group delay spectra of different resonator systems. In (ai) to (aiii), the plots in blue show the spectra at the through port of a single resonator system (i.e., only resonator 1 exists in Fig. 1) with $\kappa_2 = 0.08$, $T_1 \approx 1$. The plots in red in (ai) to (aiii) show the spectra at the through port of a twin coupled resonators system that has only one resonator directly coupled to the bus WG (i.e., $\kappa_3 = 0$ in Fig. 1) with $\kappa_1 = 0.05$, $\kappa_2 = 0.08$, $\tau_1 = \tau_2 \approx 1$. The spectra at the through port of our proposed twin coupled resonators with $\kappa_1 = 0.05$, $\kappa_2 = \kappa_3 = 0.08$, and $\tau_1 = \tau_2 = 1$ are shown in (bi) to (biii), while those at the reflection port are shown in (ci) to (ciii).

$$\xi_T = \frac{[-2r^2\cos(2\delta) + 4rr_1(r^2+1)\cos(\delta) - 2r_1^2(r^4+1) + r^2(r^2-4) + 1]}{\exp(-j\delta)\{4rr_1[r^2\exp(j\delta) + \exp(-j\delta)] - [r^4\exp(2j\delta) + \exp(-2j\delta)] - 2r^2[1+2r_1^2]\}},$$
$$\xi_R = \frac{2j\{[\cos(2\delta) - 2\cos^2(\delta)]r^2 + [2r^2 - r^4 - 1]r_1^2 - r^2 + r^4 + 1\}\{2r\cos(\delta) - r^2r_1 - r_1\}}{\exp(-j\delta)[r^2\exp(j\delta) + \exp(-j\delta) - 2rr_1]^2[1-r_1^2]^{1/2}[1-r^2]}. \quad (12)$$

For ξ_q ($q = T$ or R) in Eq. (12), four eigenmodes, which we will denote as $\delta_{1,1}$, $\delta_{1,2}$, $\delta_{2,1}$, and $\delta_{2,2}$, are formed. Consequently, as illustrated in Figs. 2(bi) and 2(ci), there are now two (four) sharp peaks and four (two) sharp dips in the transmission spectra of the through (reflection) port due to the newly formed split modes $\delta_{1,1}$, $\delta_{1,2}$, $\delta_{2,1}$, and $\delta_{2,2}$. These are in contrast to the earlier mentioned cases of $\kappa_3 = 0$ (i.e., dotted curves of Fig. 2(a)), in which there are only two split modes δ_1 and δ_2. The new split modes $\delta_{1,1}$, $\delta_{1,2}$, $\delta_{2,1}$, and $\delta_{2,2}$ in Figs. 2(bi) and 2(ci) can be described as

$$\begin{aligned}
\delta_{1,1} &\approx \delta_1 - \kappa^2/2 = \delta_0 - \sin^{-1}\kappa_1 - \kappa^2/2,\\
\delta_{1,2}/\delta_1 + \kappa^2/2 &= \delta_0 - \sin^{-1}\kappa_1 + \kappa^2/2,\\
\delta_{2,1} &\approx \delta_2 - \kappa^2/2 = \delta_0 + \sin^{-1}\kappa_1 - \kappa^2/2,\\
\delta_{2,2} &\approx \delta_2 + \kappa^2/2 = \delta_0 + \sin^{-1}\kappa_1 + \kappa^2/2. \quad (13)
\end{aligned}$$

It is evident from Eq. (13) that κ controls the formation of the multipeaks (dips) that appear in the transmission T_q spectra of the reflection (through) ports. For practical SL applications, the multipeaks and dips must be flattened. It is generally not possible to simultaneously flatten both the transmission T_q and group delay $t_{g,q}$ spectra of any MR system due to its Hilbert transform properties [12]. Nonetheless, the group delay dispersion (GDD) of our device is found to be minimal when the T_q spectrum is maximally flat. Thus, in this work, we define flat-band SL as one with (1) flat-band T_q, (2) $T_q \approx 1$, and (3) minimal GDD (i.e., close to flat-band t_g). To achieve such flat-band SL at both ports of our device, one only needs to control the mode splitting via Eq. (13) such that the multipeaks of the various split modes become undistinguishable and merge into one single broadened peak that is maximally flat at $\delta = 2\pi m$ in the resonance spectra, while at the same time producing $T_q \approx 1$. This is intuitively shown in Fig. 3: the multipeaks move inwards (in the direction of the arrows) and merge into one single, flattened peak as κ_1 is progressively decreased. The initial effective phase shift of the two (four) π swings converges into one single 2π (4π) for the through (reflection) port when flat-band SL is achieved. In the next section, we look into the conditions needed to achieve flat-band SL.

B. Optimization for Flat-Band SL

From Fig. 2(a), one can observe that, at the through port, there are two peaks (i.e., δ_1 and δ_2), while at the reflection port, there are four peaks (i.e., $\delta_{1,1}$, $\delta_{1,2}$, $\delta_{2,1}$, and $\delta_{2,2}$). Flat-band SL for the proposed twin coupled MRs can be generated at the through port if the two peaks of δ_1 and δ_2 are converted into a single flattened peak at $\delta = 2\pi m$. This means

$$\begin{aligned}
&\delta_1 = \delta_2 = \delta_0 = 2\pi m, \qquad \delta_{1,1} = \delta_{2,1} \approx 2\pi m - \kappa^2/2,\\
&\delta_{1,2} = \delta_{2,2} \approx 2\pi m + \kappa^2/2. \quad (14)
\end{aligned}$$

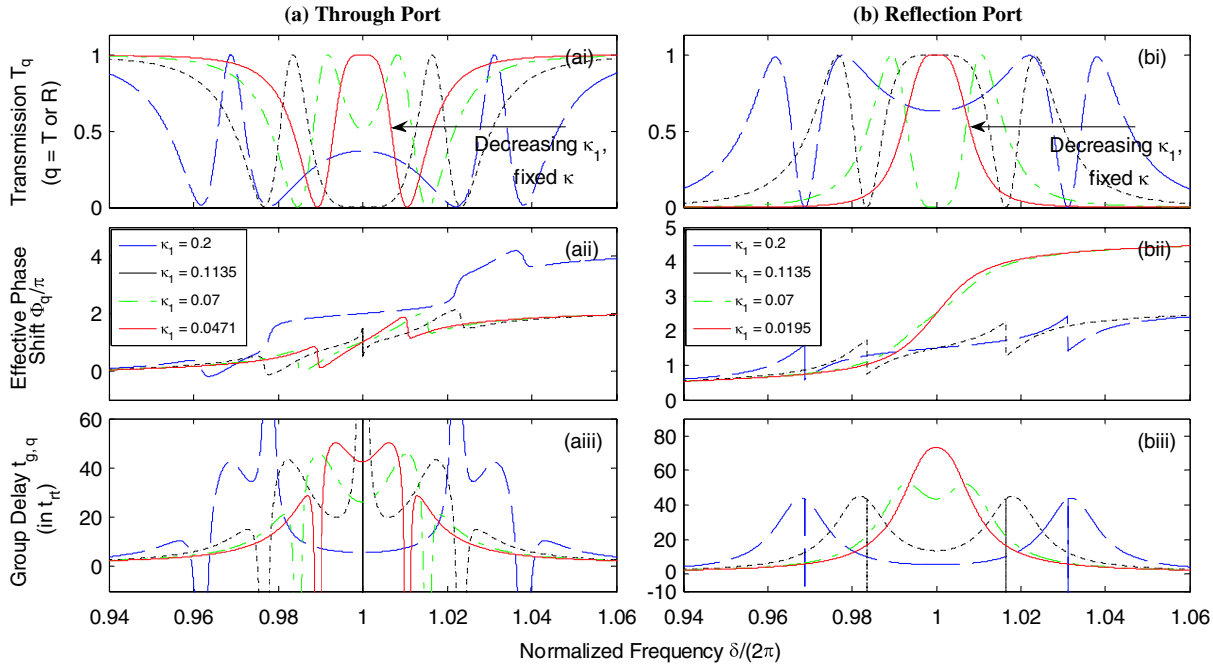

Fig. 3. (Color online) Evolution in the resonance spectra towards flat-band SL for the proposed device with $\kappa_2 = \kappa_3 = \kappa = 0.3$ as κ_1 is decreased progressively. Note that the horizontal arrows point in the direction of decreasing κ. Resonance spectra at the through port are shown in (ai) to (aiii), while those at the reflection port are shown in (bi) to (biii).

Likewise, at the reflection port, flat-band SL occurs when the four peaks of $\delta_{1,1}$, $\delta_{1,2}$, $\delta_{2,1}$, and $\delta_{2,2}$ are converted into a single flattened peak at $\delta = 2\pi m$. This means

$$\delta_1 = \delta_2 = \delta_{1,1} = \delta_{1,2} = \delta_{2,1} = \delta_{2,2} = \delta_0 = 2\pi m. \tag{15}$$

Solving Eqs. (14) and (15) together with the condition that $\partial^2|\xi_q(\delta_0)|/\partial\delta^2 = 0$ gives

$$\kappa_{s,T} = \kappa_1 = \frac{\kappa^2}{2-\kappa^2}, \quad \kappa_{s,R} = \kappa_1 = \frac{2^{-1/2}\kappa^2}{2-\kappa^2+\sqrt{2(1-\kappa^2)}}, \tag{16}$$

where $\kappa_{s,T}$ and $\kappa_{s,R}$ are the values of κ_1 needed to achieve flat-band SL at the through port and the reflection port, respectively. Using Eq. (16), we have plotted the different (κ_1, κ) needed to achieve flat-band SL in Fig. 4. It can be seen that, for both ports, $\kappa > \kappa_1$ is required for flat-band SL. The value of κ_1 needed for flat-band SL at the through port is larger than that of the reflection port, given the same κ. This means $\kappa_{s,T} > \kappa_{s,R}$, with $\kappa_{s,T} = \Psi$, where $\Psi = 2^{1/2} + 2r/(1+r^2)$. In general, $\kappa_{s,T} \approx 2.4\kappa_{s,R}$ for $\kappa < \sim 0.7$ (cf. Fig. 4).

Using different (κ_1, κ) from Fig. 4, the resonance spectra are then plotted in Fig. 5 for both ports. It is evident that maximally flat transmission T_q spectra, which are centered at $\delta = 2\pi m$, can be achieved with $T_q \approx 1$ and minimal GDD by controlling κ_1 in relation to κ. The bandwidth of the flat-band SL increases with κ, albeit smaller group delay as DBP ≈ constant. This characteristic of the DBP ≈ constant can also be verified in the effective phase shift responses in Figs. 5(aii) and 5(bii): for all (κ_1, κ), there is a fixed phase swing of $\sim 2\pi$ ($\sim 4\pi$) for the through (reflection) port. We can then deduce that the DBP of our proposed device for the through (reflection) port is $2/\pi$ ($4/\pi$). Thus, the DBPs of our proposed device will outperform other MR-based SL systems (cf. Table 1).

4. CHARACTERIZING THE FLAT-BAND SLOW LIGHT

We now characterize the flat-band SL in terms of the maximum group delay at resonance $t_{gm,q}$ and the usable resonance bandwidth $\Delta f_{u,q}$ ($q = T$ or R), where the subscript $T(R)$ denotes the through (reflection) port. We define $t_{gm,q}$ and $\Delta f_{u,q}$ as $t_{gm,q} = t'_{gm,q} \times t_{rt}$ and $\Delta f_{u,q} = \mathrm{FSR} \times \Delta\delta_{u,q}/(2\pi)$, respectively, where $t'_{gm,q}$ is the normalized group delay, $t_{rt} = 1/\mathrm{FSR}$ is the cavity round-trip time, $\mathrm{FSR} = c/(n_g L_c)$ is the free spectral range (in Hz), n_g is the group effective index, L_c is the length of the cavity, and $\Delta\delta_{u,q}$ is the normalized usable bandwidth of the flat-band SL that has maximally flat transmission T_q and minimal GDD. Using Eqs. (11)–(16), $t'_{gm,q}$ for the two output ports can be expressed as

$$t'_{gm,T} = \frac{3+r^2}{(1-r^2)}t_{rt}, \qquad t'_{gm,R} = \frac{rB^{1/2}+r^2-3}{rB^{1/2}-r^2-1}t_{rt}, \tag{17}$$

where $B = 4 - 2(1-r^2)^2/[(r^2+1+2^{1/2}r)^2]$. Using Eqs. (11)–(16), $\Delta\delta_{u,q}$ can be written as

$$\Delta\delta_{u,T} \approx \sin^{-1}\left[\frac{\kappa^2}{2}\sqrt{\frac{1}{r(2-\kappa^2)}}\right],$$
$$\Delta\delta_{u,R} \approx \frac{4}{3}\sin^{-1}\left[\frac{\kappa^2}{2}\sqrt{\frac{1}{r\left(2+r\sqrt{2}-\kappa^2\right)}}\right]. \tag{18}$$

Note that values of κ_1 and r_1 for Eqs. (17) and (18) can be found via Eq. (16). Using Eqs. (17) and (18), we have plotted $t_{gm,q}$ and $\Delta\delta_{u,q}$ of the flat-band SL in Fig. 6. The DBPs are shown in the inset in Fig. 6. Using Fig. 6, tunable flat-band SL can be realized by tuning the coupling coefficients κ and κ_1. Active tunability of κ and κ_1 is possible by using microelectromechanical systems [22] or other active tuning schemes [23], while passive tunability of κ and κ_1 (useful when it is complicated and/or costly to realize active devices) can be achieved

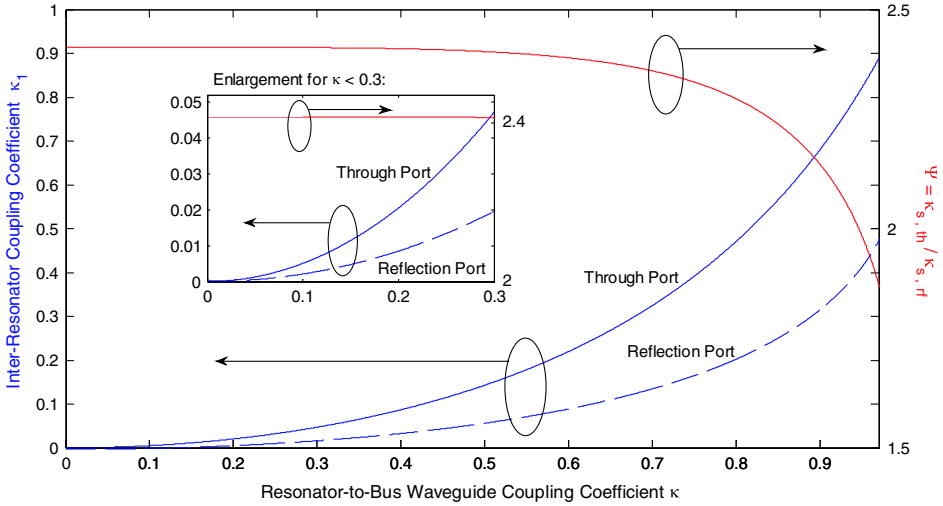

Fig. 4. (Color online) Combinations of κ_1 and κ needed for flat-band SL at the through and reflection ports of our device. The ratio $\Psi = k_{s,T}/\kappa_{s,R}$ is also shown, where $\kappa_{s,T}$ and $\kappa_{s,R}$ are the values of κ_1 that give flat-band SL at the through port and the reflection ports, respectively, for a given κ. Note that $\kappa = \kappa_2 = \kappa_3$.

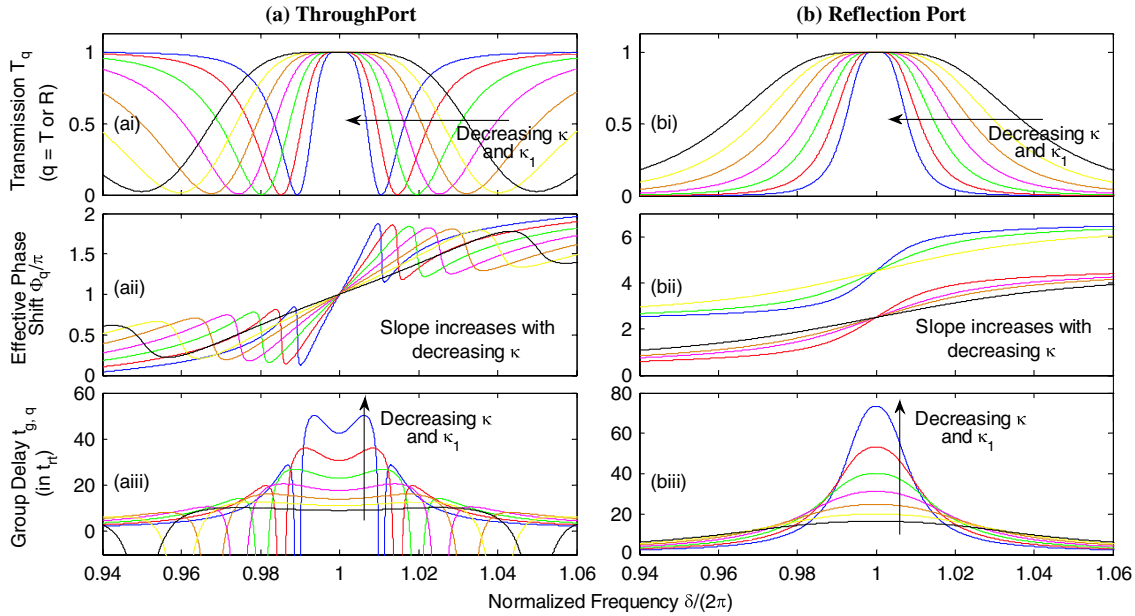

Fig. 5. (Color online) Demonstration of tunable flat-band SL for the proposed device for different κ_1 and κ. The resonance spectra at the through port are shown in (ai) to (aiii), while the resonance spectra at the reflection port are shown in (bi) to (biii). The used values of κ are $\kappa = 0.3$ (blue plots), $\kappa = 0.35$ (red plots), $\kappa = 0.4$ (green plots), $\kappa = 0.45$ (pink plots), $\kappa = 0.5$ (brown plots), $\kappa = 0.55$ (yellow plots), and $\kappa = 0.6$ (black plots). Note that the horizontal arrows point in the direction of decreasing κ and corresponding values of κ_1 used can be found from Fig. 4.

by designing different lithography masks. Some general points with regard to Fig. 6 are summarized below.

Firstly, for both ports, $t'_{gm,q}$ and $\Delta\delta_{u,q}$ share an inverse relationship: $t'_{gm,q}$ increases with decreasing κ, while $\Delta\delta_{u,q}$ increases with increasing κ. Thus, a trade-off exists between $t'_{gm,q}$ and $\Delta\delta_{u,q}$. One needs to decide whether a large $t'_{gm,q}$ or $\Delta\delta_{u,q}$ is needed for the intended SL applications, as it is not possible to achieve both. Secondly, the DBP of the through (reflection) port stays rather constant at ~0.6 (~1.3). This matches closely with our earlier deduction of DBP $= 2/\pi$ (DBP $= 4/\pi$) for the through (reflection) port. A rather constant DBP results in the above-mentioned inverse relationship between $t'_{gm,q}$ and $\Delta\delta_{u,q}$.

The actual group delay t_{gm} and actual usable bandwidth Δf_u depend on the cavity length L_c and the coupling values κ and κ_1. For a circular microring resonator (MRR) that has $L_c = 2\pi R$ (R is the bend radius) and is based on silicon-on-insulator (SOI) channel WG with width and height of 0.5 μm, using $(\kappa, \kappa_1) = (0.3, 0.0195)$ in Fig. 6 at $R = 6$ μm will translate into flat-band SL with $t_{gm} \approx 46$ ps and $\Delta f_u \approx 10$ GHz at the reflection port, while using $(\kappa, \kappa_1) = (0.5, 0.0594)$ in Fig. 6 will give SL with $t_{gm} \approx 16$ ps and $\Delta f_u \approx 26$ GHz at the same port and R. Thus, the actual group delay (bandwidth) decreases (increases) with κ. However, if a smaller R of 2 μm is used for the above MRR, $(\kappa, \kappa_1) = (0.5, 0.0594)$ in Fig. 6 will translate into flat-band SL with $t_{gm} \approx 6$ ps and $\Delta f_u \approx 78$ GHz at

Table 1. Comparison of the DBPs Between Different Traveling-Wave MR-based SL Schemes

	Conventional MR-based systems of N-cavities or unit cells in literature			This work	
	Resonance enhancement-based scheme				
Type of MR-based SL schemes	System A: N-cavities-1-bus configuration[a] [3,4,12–14]	System B: N-cavities-2-buses configuration[b] [5,6,15,16]	System C: Coupled-resonator-induced transparency-based scheme [8–11,17,18]	Output light at through port	Output light at reflection port
DBPs	$\ll 2/\pi$	$\ll 1/(2\pi)$	$\ll 1/\pi$	$\approx 2/\pi$(or ≈ 0.637) Improvement of 3-fold, 12-fold, and 6-fold as compared, respectively, to the DBPs of systems A, B, and C.	$\approx 4/\pi$(or ≈ 1.273) Improvement of 6-fold, 24-fold, and 12-fold as compared, respectively, to the DBPs of systems A, B, and C.
	Assuming that only 1/3 of the FWHM is the usable resonance bandwidth in order to avoid higher-order dispersion:				
	≈ 0.212	≈ 0.0531	≈ 0.106		

[a] N-cavities-1-bus configuration: a chain of N-resonators coupled to one bus WG. This is also known as the all-pass filter configuration if all the cavities are lossless.
[b] N-cavities-2-buses configuration: a chain of N-resonators coupled to two bus WGs. This is also known as the add-drop filter configuration. Note that $N(= 1, 2, 3\ldots)$ is the number of resonators.

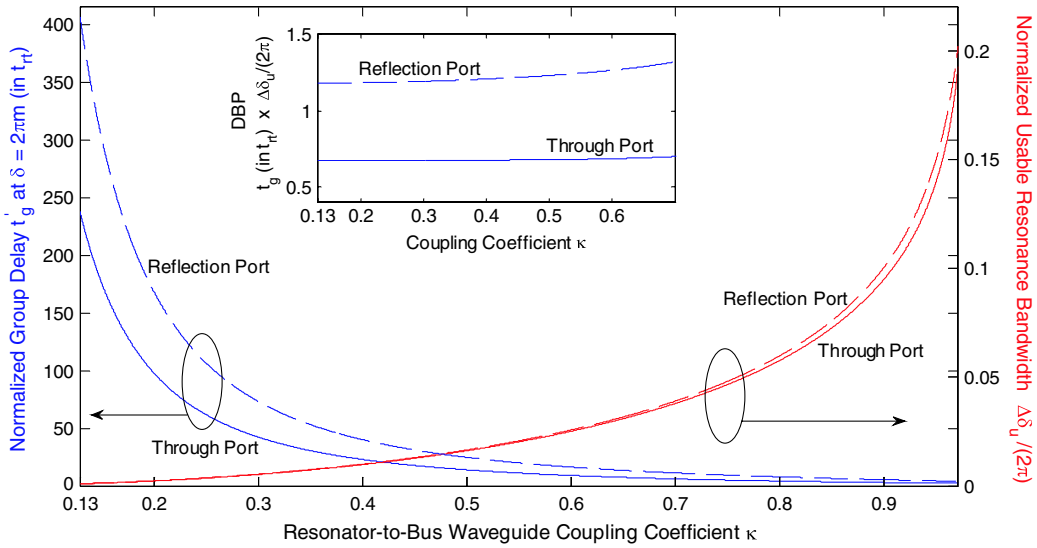

Fig. 6. (Color online) The normalized group delay (left axis) and the normalized usable resonance bandwidth (right axis) of the flat-band SL for the through port (solid curves) and reflection port (dotted curves) of the proposed device at different κ. Corresponding values of κ_1 can be found in Fig. 4. The inset shows the DBP.

the reflection port. Thus, a smaller R gives a larger Δf_u but at a trade-off of a smaller t_{gm}. A compromise must therefore be reached depending on whether a large Δf_u or t_{gm} is needed. Note that if a racetrack MRR is used instead of a circular MRR, t_{gm} will be larger albeit a smaller Δf_u. We will thus focus on circular MRRs for the rest of this work.

5. EFFECTS OF FABRICATION ERRORS AND CAVITY LOSSES

The performances of our proposed device after fabrication will chiefly depend on (1) the fabrication tolerance and (2) the cavity losses. It is found that the flat-band SL of our device is relatively unaffected if fabrication errors in the WG and cavity dimensions are about $\pm 1\%$. To date, deep UV lithography has made it possible to control the WG dimensions to within $\pm 1\%$ [24] for SOI-based MRRs. Hence, fabrication tolerance is not much of an issue for our proposed scheme. On the other hand, cavity losses, which consist of the propagation and coupler losses, are expected to be the dominant sources of degradation to the SL performances of our proposed device. These are discussed below.

A. Propagation Losses

In MRRs, the chief components of the propagation losses are the fabrication-induced sidewall roughness losses and the bend losses. The bend losses are the main source of the propagation losses, as the fabrication-induced sidewall roughness

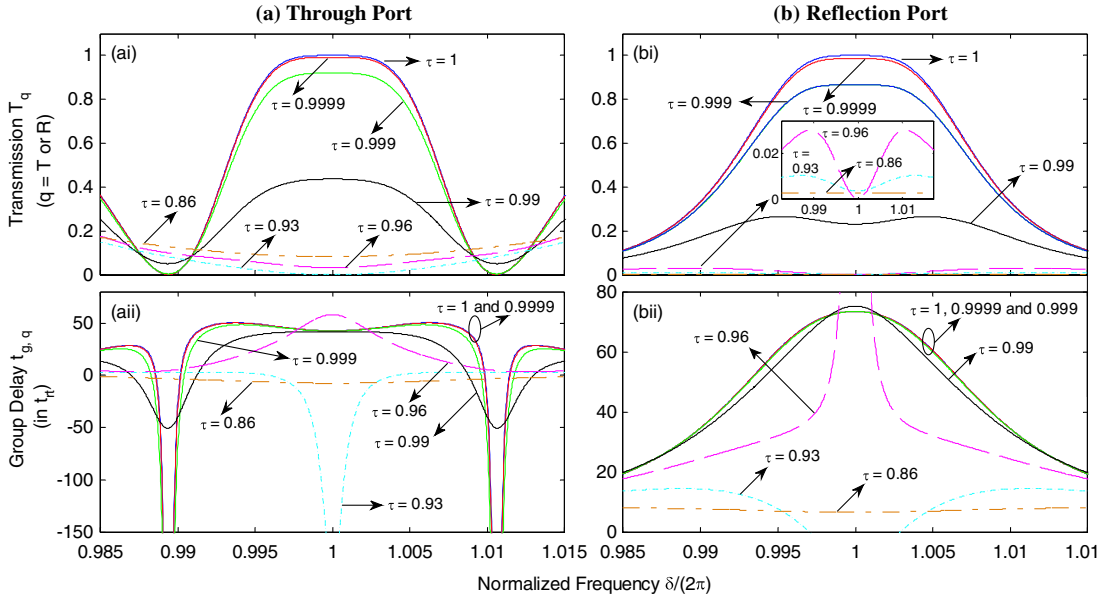

Fig. 7. (Color online) The effects of cavity losses on the transmission T_q and group delay $t_{g,q}$ spectra of the flat-band SL at the (ai)–(aii) through port and the (bi)–(bii) reflection port of the proposed device with $(\kappa, \kappa_1) = (0.3, 0.0471)$ for the through port and $(\kappa, \kappa_1) = (0.3, 0.0195)$ for the reflection port.

can easily be reduced to a negligible level [25]. The propagation losses of each MRR are quantified by τ_n. As $\delta_1 = \delta_2 = \delta$ in this work, we use $\tau_1 = \tau_2 = \tau$ ($\tau < 1$, net optical loss; $\tau = 1$, zero optical loss).

Let us first look at the effects of varying τ (assuming no coupler loss) on the flat-band SL for one particular example of $\kappa = 0.3$ for our proposed device (with value of κ_1 from Fig. 4). It can be seen in Fig. 7 that flat-band SL with close to unity transmission ($T_q \approx 1$) can be realized at both ports provided that $0.9999 \le \tau \le 1$. For such small losses of $0.9999 \le \tau \le 1$, the group delay of the flat-band region (at $\delta = 2\pi m$) of the flat-band region is rather independent of τ. Increasing the losses to $\tau < 0.9999$ results in the transmission falling considerably below $T_q = 1$, while the group delay remains fairly unaffected as long as τ does not fall considerably below $\tau < 0.999$. To relax the fabrication constraints, we will consider devices with transmissions of $0.8 \le T_q \le 1$.

The general characteristics as seen in Fig. 7 apply to any value of κ. However, the range of values of τ that gives flat-band SL changes with κ. To illustrate this, we have shown the transmission T_q and group delay responses at $\delta = 2\pi m$ of our device as a function of τ for different κ (with values of κ_1 from Fig. 4) in Fig. 8. It can be observed that there are specific values of τ that give points of asymptote in the group delay responses, with corresponding points of $T_q = 0$ in the transmission responses. This phenomenon of $T_q = 0$ that is accompanied by a sharp change in the group delay for resonator systems is generally known as critical coupling. We will term the values of τ that give such phenomenon as τ_c. The value of τ_c (cf. points of asymptote and $T_q = 0$ in Fig. 8) decreases with increasing κ. As a result, the transmission T_q and group delay near the points corresponding to $T_q \approx 1$ become less sensitive to changes in τ at large κ. Generally, the group delay is less sensitive to changes in τ than the transmission, consistent with Fig. 7. For both the through and reflection ports, the group delay is fairly constant (cf. insets in Fig. 8(aii) and 8(bii)) for all κ if τ is in the range of $0.98 \le \tau \le 1$. On the other hand, to have high transmission of $0.8 \le T_q \le 1$ (cf. insets in Fig. 8(ai) and 8(bi)) for both ports and all κ, the allowed range of τ reduces to $\sim 0.999 \le \tau \le 1$.

Theoretically speaking, it is possible to achieve the above range of $\sim 0.999 \le \tau \le 1$ for a passive MRR with bend radius R of $R \ge 2$ μm if SOI wires are used [26]. Moreover, it has been experimentally demonstrated that $\tau \approx 0.989$ can be achieved for a passive SOI-based MRR with $R = 1.0$ μm [27]. This implies the technical possibility to realize $\sim 0.999 \le \tau \le 1$ for an SOI-based MRR with $R \ge 2$ μm as τ increases exponentially with R.

B. Coupler Losses

Besides the propagation losses, the coupler losses of the MRRs would also influence the flat-band SL. The coupler loss at each CJ is characterized by σ_i (lossless coupler: $\sigma_i = 0$). For simplicity, we assume equal coupler losses at all the CJs; i.e., $\sigma_1 = \sigma_1 = \sigma_3 = \sigma$. We also set $\tau = 0.999$ in this section, as it has been concluded in Subsection 5.A that to realize flat-band SL with high transmission, τ must be at least ~ 0.999.

The effects of varying σ on the flat-band SL of the proposed device is shown in Fig. 9 for the case of $\kappa = 0.3$ (with values of κ_1 from Fig. 4). It is evident that for the through (reflection) port, a coupler loss of $\sigma \le \sim 0.04$ ($\sigma \le \sim 0.02$) at each CJ will keep the transmission of the flat-band SL (at $\delta = 2\pi m$) to a high level of $0.8 \le T_q \le 1$. The group delay at $\delta = 2\pi m$, on the other hand, is relatively independent of the coupler losses.

The general characteristics as seen in Fig. 9 apply to any value of κ. However, the range of values of τ that gives flat-band SL changes with κ. To illustrate this, we have shown the transmission T_q and group delay responses at $\delta = 2\pi m$ of our device as a function of τ for different κ (with values of κ_1 from Fig. 4) in Fig. 10. It can be seen from Figs. 10(ai) and 10(bi) that, for each value of κ, the transmission T_q decreases

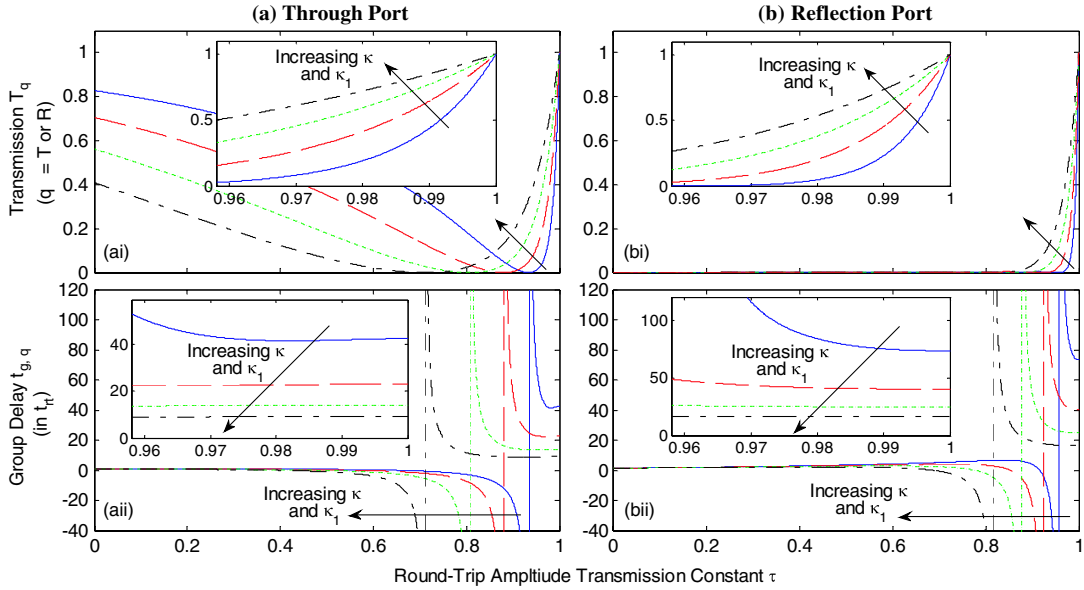

Fig. 8. (Color online) The effects of cavity losses on the transmission T_q and group delay $t_{g,q}$ of the flat-band SL at $\delta = 2\pi m$ for the (ai)–(aii) through port and (bi)–(bii) reflection port of our device for different κ_1 and κ. The used values of κ are $\kappa = 0.3$ (blue plots), $\kappa = 0.4$ (red plots), $\kappa = 0.5$ (green plots), and $\kappa = 0.6$ (black plots). Note that the horizontal arrows point in the direction of increasing κ and corresponding values of κ_1 can be found in Fig. 4.

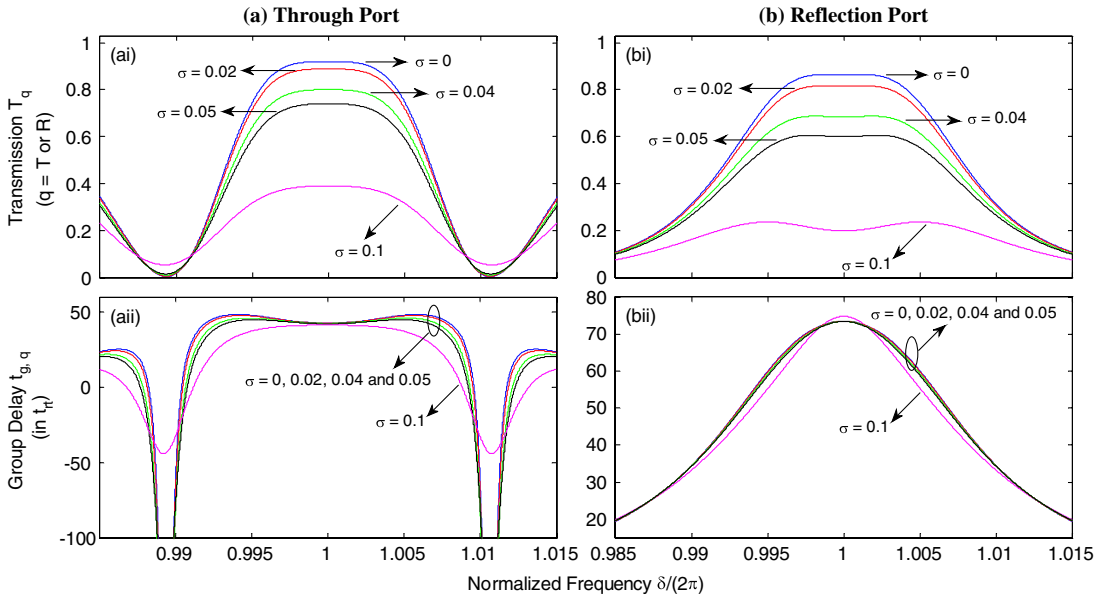

Fig. 9. (Color online) The effects of varying coupler losses on the transmission T_q and group delay t_g,q spectra of the flat-band SL at the (ai)–(aii) through port and the (bi)–(bii) reflection port of the proposed device with $(\kappa, \kappa_1) = (0.3, 0.471)$ for the through port and $(\kappa, \kappa_1) = (0.3, 0.0195)$ for the reflection port. Propagating loss of each cavity is fixed at $\tau = 0.999$.

with increasing σ until the critical coupling point (in which $T_q = 0$) is reached. We will term the value of σ that gives critical coupling as σ_c. Such a critical coupling point is reflected as an asymptote in the group delay spectra in Figs. 10(aii) and 10(bii). In general, σ_c increases with κ. Consequently, the transmission T_q and group delay near the points corresponding to $T_q \approx 1$ become less sensitive to changes in σ at larger κ. Also, as shown in Fig. 10, the group delay is less sensitive to changes in σ than the transmission. For both the through and reflection ports, the group delay is fairly constant for all κ provided that $\sigma \leq \sim 0.1$. However, to achieve flat-band SL with high transmission of $0.8 \leq T_q \leq 1$ for both ports, the allowed range of σ will decrease to $\sigma \leq \sim 0.02$ so that all values of κ can be utilized.

It is found that for an SOI-based circular MRR, σ at each CJ is $\sigma < \sim 0.01$ for bend radius $R \geq 1$ μm [27]. This implies that the effects of coupler losses on the flat-band SL of our device are negligible as $\sigma \leq \sim 0.02$ for our proposed scheme, as mentioned above. Based on the results in Subsections 5.A and 5.B, we can conclude that our proposed scheme is suitable for practical SL applications when a circular SOI-based MRR is being used.

Finally, note that the fact that the ranges of $\sim 0.999 \leq \tau \leq 1$ (cf. Subsection 5.A) and $\sigma \leq \sim 0.02$ (this section) give flat-band

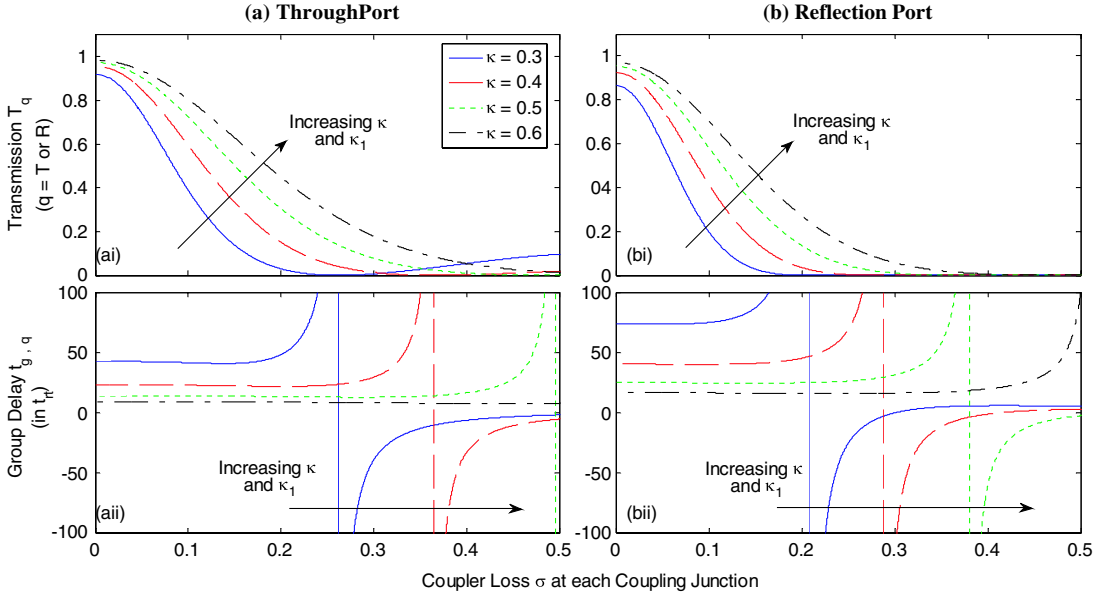

Fig. 10. (Color online) The effects of coupler losses on the transmission T_q and group delay $t_{g,q}$ of the flat-band SL at $\delta = 2\pi m$ for the (ai)–(aii) through port and the (bi)–(bii) reflection port of our device for different κ_1 and κ. The used values of κ are $\kappa = 0.3$ (blue plots), $\kappa = 0.4$ (red plots), $\kappa = 0.5$ (green plots), and $\kappa = 0.6$ (black plots). Note that the horizontal arrows point in the direction of increasing κ and corresponding values of κ_1 used for each port can be found in Fig. 4.

SL with high transmission does not conflict with the well-known Kramers–Kronig relation [2]. As mentioned in [28], for MR structures, the Kramers–Kronig relation exists only in the under-coupling regime. However, the above-mentioned ranges of $\sim 0.999 \leq \tau \leq 1$ and $\sigma \leq \sim 0.02$ will cause our proposed MR structure to be in the over-coupling regime. This produces SL [6], which has been demonstrated in this work.

6. SUMMARY AND CONCLUSIONS

We have proposed a twin coupled traveling-wave MRs scheme to generate flat-band SL at both the through and reflection ports. Such flat-band SL has (1) maximally flat transmission spectrum, (2) high transmission, (3) minimal GDD, (4) enhanced DBPs that are 3- to 24-fold (cf. Table 1) higher than conventional SL systems [3–6,8–18], and (5) tunable bandwidth and group delay (by adjusting the coupling coefficients). It is also found that the fabrication errors in the WG dimensions must be kept within $\pm 1\%$ and that the size of the bend radius R should be $R \geq 2$ μm so that the flat-band SL is not severely degraded. These can be achieved as advancement in fabrication technology has allowed a fabrication tolerance of $\pm 1\%$ [24] and low-loss MRs with R as small as 1 μm [27] to be fabricated. Our proposed device will, therefore, be suitable for practical SL applications.

REFERENCES

1. D. Gauthier, "Slow light brings faster communication," Phys. World **18**, 30–32 (2005).
2. P. W. Milonni, *Fast Light, Slow Light and Left-Handed Light* (Taylor & Francis, 2004).
3. K. Totsuka and M. Tomita, "Dynamics of fast and slow light propagation through a microsphere-optical-fiber-system," Phys. Rev. E **75**, 6610–6614 (2007).
4. H. P. Uranus, L. Zhuang, C. G. H. Roeloffzen, and M. H. J. W. Hoekstra, "Pulse advancement and delay in an integrated-optical two-port ring-resonator circuit: direct experimental observations," Opt. Lett. **32**, 2620–2622 (2007).
5. O. Schwelb, "Transmission, group delay, and dispersion in single-ring optical resonators and add/drop filters-a tutorial overview," J. Lightwave Technol. **22**, 1380–1394 (2004).
6. T. Y. L. Ang and N. Q. Ngo, "Harnessing coupler-induced localized backscattering for enhanced fast and slow light performances in a traveling wave microresonator," J. Opt. Soc. Am. B **27**, 2639–2647 (2010).
7. L. V. Hau, S. E. Harris, Z. Dutton, and C. H. Behroozi, "Light speed reduction to 17 metres per second in an ultracold atomic gas," Nature **397**, 594–598 (1999).
8. D. D. Smith, H. Chang, K. A. Fuller, A. T. Rosenberger, and R. W. Boyd, "Coupled-resonator-induced transparency," Phys. Rev. A **69**, 063804 (2004).
9. L. Maleki, A. B. Matsko, A. A. Savchenkov, and V. S. Ilchenko, "Tunable delay line with interacting whispering-gallery-mode resonators," Opt. Lett. **29**, 626–628 (2004).
10. K. Totsuka, N. Kobayashi, and M. Tomita, "Slow light in coupled-resonator-induced transparency," Phys. Rev. Lett. **98**, 213904 (2007).
11. M. Tomita, K. Totsuka, R. Hanamura, and T. Matsumoto, "Tunable Fano interference effect in coupled-microsphere resonator-induced transparency," J. Opt. Soc. Am. B **26**, 813–818 (2009).
12. G. Lenz, B. J. Eggleton, C. K. Madsen, and R. E. Slusher, "Optical delay lines based on optical filters," IEEE J. Quantum Electron. **37**, 525–532 (2001).
13. C. G. H. Roeloffzen, L. Zhuang, R. G. Heideman, A. Borreman, and W. van Etten, "Ring resonator-based tunable optical delay line in LPCVD waveguide technology," in *Proc. IEEE/LEOS Benelux Chapter, 10th Symp* (2005), 71–74.
14. F. Xia, L. Sekaric, and Y. Vlasov, "Ultracompact optical buffers on a silicon chip," Nature **1**, 65 (2007).
15. J. K. S. Poon, J. Scheuer, Y. Xu, and A. Yariv, "Designing coupled-resonator optical waveguide delay lines," J. Opt. Soc. Am. B **21**, 1665–1673 (2004).
16. F. Xia, L. Sekaric, M. O'Boyle, and Y. Vlasov, "Coupled resonator optical waveguides based on silicon-on-insulator photonic wires," Appl. Phys. Lett. **89**, 041122 (2006).
17. Y. F. Xiao, X. B. Zou, W. Jiang, Y. L. Chen, and G. C. Guo, "Analog to multiple electromagnetically induced transparency in all-optical drop-filter systems," Phys. Rev. A **75**, 063833 (2007).
18. M. Mancinelli, R. Guider, P. Bettotti, M. Masi, M. R. Vanacharla, and L. Pavesi, "Coupled-resonator-induced-transparency concept for wavelength routing applications," Opt. Express **19**, 12227–12240 (2011).
19. Y. Chung, D. G. Kim, and N. Dagli, "Reflection properties of coupled-ring reflectors," J. Lightwave Technol. **24**, 1865–1874 (2006).
20. I. Chremmos and N. Uzunoglu, "Reflective properties of double-ring resonator system coupled to a waveguide," IEEE Photon. Technol. Lett. **17**, 2110–2112 (2005).
21. L. Y. Mario and M. K. Chin, "Optical buffer with higher delay-bandwidth product in a two-ring system," Opt. Express **16**, 1796–1807 (2008).
22. J. Yao, D. Leuenberger, M. C. M. Lee, and M. C. Wu, "Silicon microtoroidal resonators with integrated MEMS tunable coupler," IEEE J. Sel. Top. Quantum Electron. **13**, 202–208 (2007).
23. A. H. Atabaki, B. Momeni, A. A. Eftekhar, E. S. Hosseini, S. Yegnanarayanan, and A. Adibi, "Tuning of resonance-spacing in a traveling-wave resonator device," Opt. Express **18**, 9447–9455 (2010).
24. W. Bogaerts, L. Liu, S. Selvaraja, J. Brouckaert, D. Taillaert, D. Vermeulen, G. Roelkens, D. Van Thourhout, and R. Baets, "Silicon nanophotonic waveguides and their applications," Proc. SPIE **7134**, 71341O (2008).
25. D. K. Sparacin, S. J. Spector, and L. C. Kimerling, "Silicon waveguide sidewall smoothing by wet chemical oxidation," J. Lightwave Technol. **23**, 2455–2461 (2005).
26. A. M. Prabhu, A. Tsay, Z. Han, and V. Van, "Ultracompact SOI microring add-drop filter with wide bandwidth and wide FSR," IEEE Photon. Technol. Lett. **21**, 651–653 (2009).
27. A. M. Prabhu, A. Tsay, Z. Han, and V. Van, "Extreme miniaturization of silicon add-drop microring filters for VLSI photonics applications," IEEE Photon. Technol. Lett. **2**, 436–444 (2010).
28. J. Heebner, R. Grover, and T. Ibrahim, *Optical Microresonators: Theory, Fabrication, and Applications* (Springer-Verlag, 2008).